

# Stacking Faults in Co-Alloy Longitudinal Media

B. Lu, Jie Zou, David N. Lambeth, and David E. Laughlin

**Abstract**—Stacking faults in CoCrTa/Cr, CoCrPt/NiAl, and CoCrPt/Cr/NiAl films have been studied by electron diffraction. Interfacial lattice match and epitaxial growth play important roles in reducing the stacking fault density. It is found that the bicrystal media has large stacking fault densities. In the unicast media case, when good epitaxy between magnetic layer and underlayer cannot be achieved, there are many randomly oriented grains in the magnetic layer. These random grains have a high stacking fault density.

**Index Terms**—Epitaxial growth, lattice match, longitudinal media, magnetic recording media, stacking fault.

## I. INTRODUCTION

TO ALLEVIATE the thermal stability problem for longitudinal magnetic recording media, it is very important to narrow the energy barrier ( $K_u V$ ) distribution of thermal activation [1]. Compared with the study of grain size ( $V$ ) distribution by TEM imaging, the  $K_u$  distribution is difficult to study quantitatively. The dispersion of  $K_u$  is due to the variation of crystalline perfection of magnetic grains. For a medium of hcp Co-alloy, stacking faults (SF's) or fcc-like regions occur frequently because the free energy difference between hcp and fcc stacking is small and sputtering deposition is a nonequilibrium process. Any perturbation introduced by contamination [2], [3], poor-epitaxial growth [4], [5], or interfacial stress [6]–[8] may cause SF's.

It has been found that the maximum coercivity of a medium is correlated to the minimum lattice mismatch between the magnetic layer and the underlayer [8]. Although it is difficult to separate the influence of SF's on the magnetic properties from other effects such as in-plane strain, or mis-orientation, it is obvious that the fcc nature of atomic arrangements will deteriorate the magnetic hardness of hcp Co-alloy when present in high fault density [9]. It was recently demonstrated that media with high SF density also show significant magnetic viscosity effects [10], implying lower  $K_u$  and high dispersion in the  $K_u$  values.

Generally speaking, SF's can be examined by X-ray diffraction (XRD), electron diffraction (ED) and transmission electron microscopy (TEM) imaging. For longitudinal media, ideal  $c$ -axis orientation lies in media plane. In this case the SF, which are parallel to the (00.1) hcp plane, are perpendicular to the film plane. Therefore, for XRD studies, grazing-incidence with a strong synchrotron light source is the essential to characterize

SF's. In other geometry diffraction intensities from SF's are superimposed with the intensities from either substrate or underlayer. For the TEM imaging, the number of grains that can be studied at one time is limited by the magnification of the image. ED can be used to study the grains in large quantity and so with little statistical error. Moreover, since the substrate is removed during TEM specimen preparation, interference from substrate is not an issue. However it should be mentioned that the intensity of the electron diffraction is not as reliable as that of XRD due to dynamic scattering of electrons. It is difficult to distinguish the effect of growth fault and deformation fault as what can be done in XRD [11].

In this study, SF's in both bicrystal and unicast media are studied by ED. The role of the crystallographic texture and epitaxy of the underlayers with the magnetic layer is emphasized.

## II. EXPERIMENTAL PROCEDURE

Bicrystal CoCrTa/Cr films were deposited onto flat NiP/Al–Mg substrates by using dc magnetron sputtering. The substrate was preheated to 250°. Thicknesses of the CoCrTa and Cr layer are 22 nm and 60 nm respectively. No substrate bias was applied during deposition. Similarly unicast films of CoCrPt/NiAl and CoCrPt/Cr/NiAl were deposited onto Corning 7059 glass coupon by rf diode sputtering without substrate preheating but with –100 V bias. The thicknesses of the CoCrPt, NiAl and Cr layers are 30 nm, 100 nm, and 100 nm respectively. XRD  $\theta - 2\theta$  scan was performed on a Rigaku x-ray diffractometer. ED and TEM imaging was carried out with a Philips EM420 transmission electron microscope. TEM sample preparing has been reported elsewhere [12].

## III. RESULTS AND DISCUSSION

Bicrystal media has (11.0) crystallographic texture of Co-alloy film and (200) texture of Cr-alloy film, while unicast media has Co-alloy grains in (10.0) texture and Cr-alloy grains in (112) texture. Cr has a bcc lattice. The body diagonal of its unit cell is 4 times the Cr atomic radius,  $R_{Cr}$ . Hence, the lattice parameter of bcc Cr unit cell is  $a^{Cr} = 4/\sqrt{3}R_{Cr}$ . Co has a hcp lattice. Likewise, the lattice parameter of its unit cell is:  $a = 2R_{Co}$ ,  $c = \sqrt{8/3}a = 2\sqrt{8/3}R_{Co}$ , where  $R_{Co}$  is Co atomic radius. The lattice configurations of Cr(200), Co(11.0), Cr(112), and Co(10.0) planes are drawn in Fig. 1. It is obvious that the ratios of two basic lattice spacing of Cr(200) and Co(11.0) planes are 1 and 1.06, respectively. Therefore these two planes can never be perfectly matched by alloying the underlayer (CrX). However, the ratios for the Cr(112) and Co(10.0) are the same, namely  $\sqrt{8/3}$ . Consequently, by alloying the underlayer, a perfect lattice match can be achieved. Hence, it is expected that

Manuscript received February 5, 2000. This work was supported in part by the Data Storage System Center at CMU.

B. Lu, J. Zou, and D. N. Lambeth are with the Electrical and Computer Engineering Department, Carnegie Mellon University, Pittsburgh, PA 15213 USA.

D. E. Laughlin is with the Materials Science and Engineering Department, Carnegie Mellon University, Pittsburgh, PA 15213 USA.

Publisher Item Identifier S 0018-9464(00)09046-4.

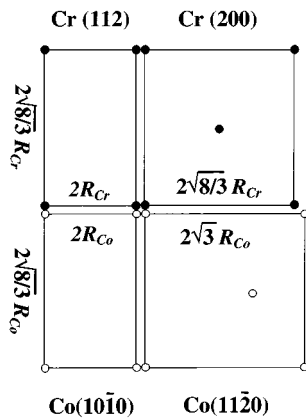


Fig. 1. Schematic diagram showing lattice configuration of Cr(200), Cr(112), Co(11.0), and Co(10.0) planes.

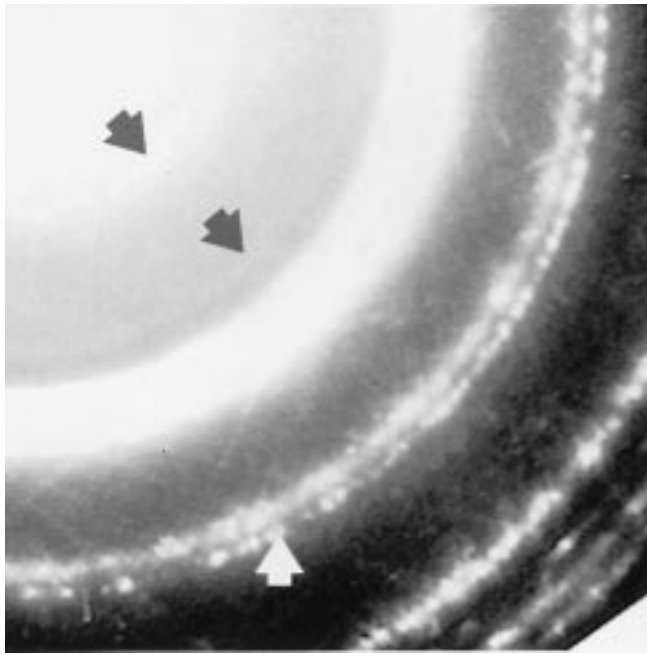


Fig. 2. Electron diffraction pattern (EDP) of CoCrTa/Cr bilayer.

the bicrystal Co-alloy films will contain more SF's than the ideal uncrystal films.

Fig. 2 shows a quadrant of electron diffraction pattern of the CoCrTa/Cr films with CoCrTa(11.0) texture and Cr(200) texture. The innermost two extra rings noted by the black arrows are due to the double diffraction of Cr(110) + Co(10.1) and Cr(110) + Co(20.0), respectively. The bright band contains kinematic diffraction rings, such as Co(10.0), Co(00.2), Cr(110), and Co(10.1), as well as double diffraction rings, like Cr(110) + Co(10.2), Cr(200) + Co(10.0), and Cr(200) + Co(00.2). The double rings noted by a white arrow are the Co(10.2) (smaller diameter) and Cr(200) rings (larger diameter).

The schematic drawing in Fig. 3 shows the first 4 diffraction rings from the CoCrTa layer. They are (10.0), (00.2), (10.1), and (10.2) from the inside out. Since the SF's are parallel to the (00.1) plane, they generate streaks along the  $[00.1]^*$  reciprocal lattice direction of each of the reflections. Consequently, the streaks are tangential to the (hk.0) rings, radial to the (00.2)

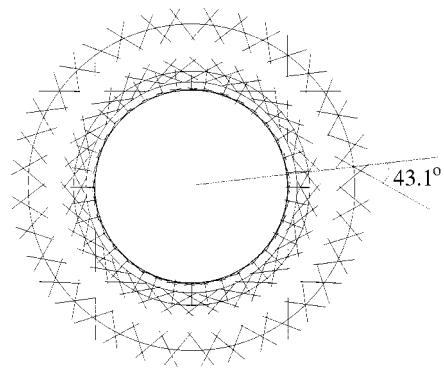


Fig. 3. Schematic diagram of the first 4 rings of CoCrTa layer in Fig. 2.

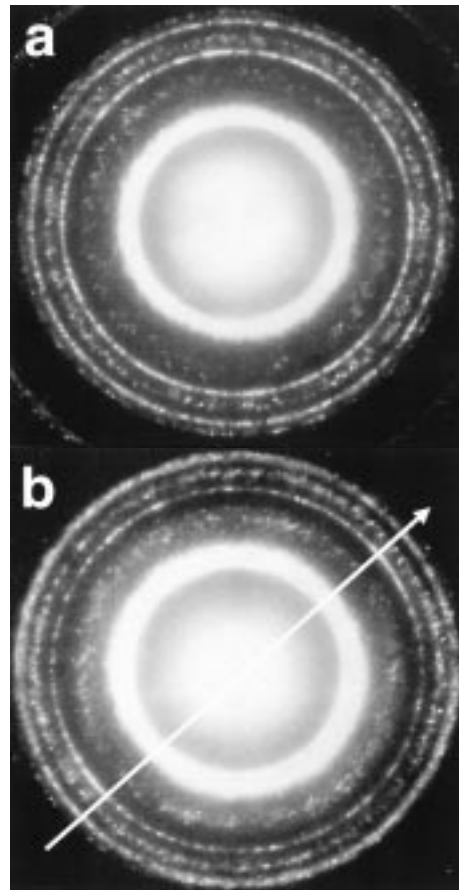


Fig. 4. EDP of CoCrPt/NiAl film. (a)  $0^\circ$  tilt, (b)  $30^\circ$  tilt.

rings,  $\pm 61.9^\circ$  to the radius of (10.1) ring and  $\pm 43.1^\circ$  to the radius of (10.2) ring, as shown in the schematic diagram.

It is very clear in the EDP in Fig. 2 that there are quantities of streaks next to the (10.1) and (10.2) rings. These streaks have fixed angles to the radius of the two rings. The angles were measured as  $59.1^\circ$  and  $-62.6^\circ$  for the (10.1) ring and as  $43.0^\circ$  and  $-44.5^\circ$  for the (10.2) ring. This confirms that the streaks are contributed by the SF's in the (11.0) textured CoCrTa grains.

Fig. 4(a) shows an EDP of the CoCrPt/NiAl films. The diffraction rings of NiAl are all present except for the (200) ring. This confirms that the top part of NiAl layer is in (112) texture [12]. Because the uncrystal grains of CoCrPt are oriented with (10.0) in film normal, only the (00.2) ring of all

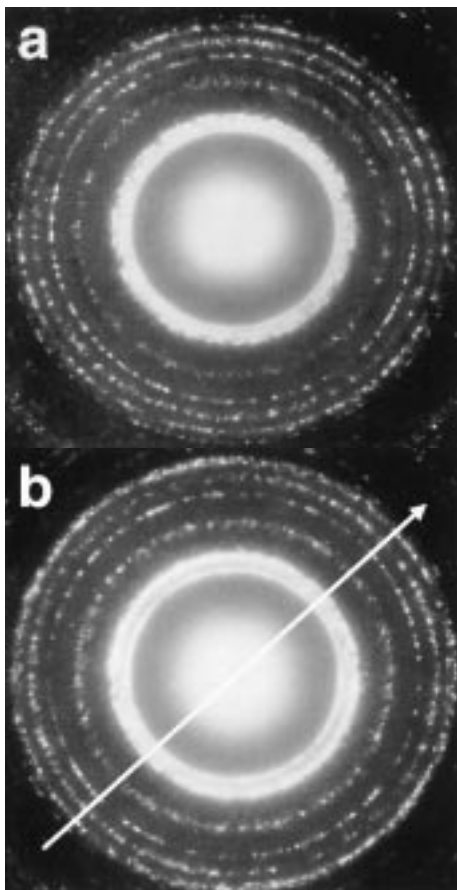


Fig. 5. EDP of CoCrPt/Cr/NiAl film. (a)  $0^\circ$  tilt, (b)  $30^\circ$  tilt.

the first four rings is able to present in the EDP. The (10.0), (10.1), (10.2) rings in Fig. 4(a) are actually contributed by randomly oriented grains, which also has contribution to the (00.2) ring. Consequently, it can be seen that the streaks next to the (10.1) and (10.2) rings are oriented randomly. Moreover, some extra spots present at the side of the (10.2) ring. These extra spots are contributed by the stacking fault of CoCrPt grains whose  $c$ -axes are almost perpendicular to the film.

Since it is impossible to see the streaks from the (10.0) textured uniaxial grains at  $0^\circ$ -tilted position, an EDP was taken at  $30^\circ$ -tilted position as shown in Fig. 4(b). The long white arrow is the tilt axis. It can be seen that two (10.2) arcs from uniaxial grains are superimposed on the (10.2) rings from randomly oriented grains. Near the arcs region it is difficult to find any long, fixed-angle streaks as observed in the EDP of the bicrystal CoCrTa (Fig. 2). This suggests that there are few SF's in the (10.0)-textured grains.

Fig. 5(a) and (b) show EDP's of the CoCrPt/Cr/NiAl films tilted at  $0^\circ$  and  $30^\circ$ , respectively. They are very similar to the EDP's in Fig. 4(a) and (b). However, it is worth noting that the intensity of the (10.2) ring and its streaks are much weaker than their counterpart in Fig. 4. This suggests that the intermediate layer Cr reduce the stacking fault density and number of randomly oriented grains in the CoCrPt layer. It was also found by

XRD  $\theta-2\theta$  scan that the (10.0) peak became stronger when the Cr intermediate layer was used.

The intermetallic bonding of B2 NiAl has component of covalent bond [13], which is directional. Because of this, it is difficult to achieve hetero-structural epitaxy between NiAl (112) and Co(10.0). On the other hand, Cr is of bcc structure, which is similar to B2 structure, in terms of atomic sites. Therefore, Cr can easily grow epitaxially on top of NiAl, in spite of the directional bond. Ref. [12] has shown that a Cr layer on top of the NiAl layer has a narrower angular distribution of (112) orientations than that of NiAl layer. It should be noted that the ED was obtained from the middle portion of the NiAl layer, but that the (112) texture evolves and improves with NiAl thickness. This indicates that Cr grains epitaxially grow on the top of the NiAl layer and pick up the better (112) orientation of the top of the NiAl layer.

Since Cr is of pure metallic bond, which is nondirectional, hcp Co can epitaxially grow on top of it with little difficulty. This epitaxy between Cr and Co has been demonstrated in the past for many years in Co/Cr bilayer media. It is therefore reasonable to expect that when well lattice matched Co-alloy/CrX/NiAl epitaxial thin films are grown the lowest SF densities will result.

#### IV. CONCLUSION

Electron diffraction is a useful and direct method to study SF's in Co-alloy longitudinal media. Interfacial lattice match and epitaxial growth has a strong influence in determining SF density of the magnetic layer.

For CoCrTa/Cr bicrystal media, which always has a large lattice misfit in at least one direction, the SF density is high. Due to the poor epitaxy between CoCrPt and NiAl layer, many randomly oriented grains exist in the CoCrPt films. A Cr intermediate layer can effectively reduce the number of randomly oriented grains through enhancing the epitaxial growth, while reducing the SF density.

#### REFERENCES

- [1] D. Weller and A. Moser, *IEEE Trans. Magn.*, vol. 35, p. 4423, 1999.
- [2] T. M. Coughlin, E. R. Wuori, and J. H. Judy, *J. Vac. Sci. Technol.*, vol. 20, p. 171, 1982.
- [3] D. J. Mapps, N. Mahvan, and M. A. Akhter, *IEEE Trans. Magn.*, vol. Mag-23, p. 2473, 1987.
- [4] K. Hono, B. G. Demczyk, and D. E. Laughlin, *Appl. Phys. Lett.*, vol. 55, p. 229, 1989.
- [5] T. P. Nolan, R. Sinclair, R. Ranjan, and T. Yamashita, *IEEE Trans. Magn.*, vol. 29, p. 292, 1993.
- [6] A. Ishikawa and R. Sinclair, *IEEE Trans. Magn.*, vol. 32, p. 3605, 1996.
- [7] B. Lu, D. E. Laughlin, and D. N. Lambeth, *Poster at TMRC'99*.
- [8] G. L. Chen, *IEEE Trans. Magn.*, vol. 34, p. 366, 1998.
- [9] N. S. Walmsley, R. W. Chantrell, and J. J. Miles, *J. Magn. Magn. Mater.*, vol. 193, p. 196, 1999.
- [10] P. Dova, H. Laidler, K. O'Grady, M. F. Toney, and M. F. Doerner, *J. Appl. Phys.*, vol. 85, p. 2775, 1999.
- [11] B. E. Warren, *X-Ray Diffraction*, New York: Dover, p. 275.
- [12] B. Lu, D. E. Laughlin, D. N. Lambeth, S. Z. Wu, R. Ranjan, and G. C. Rauch, *J. Appl. Phys.*, vol. 85, p. 4295, 1999.
- [13] Z. W. Wu, S. H. Wei, and A. Zunger, *Acta Metall. Mater.*, vol. 40, p. 2155, 1992.